Unwinding Relaxation Dynamics of Polymers

J.-C. Walter,[1,2] M. Baiesi,[3,4] G. T. Barkema,[5,1] and E. Carlon[2]

[1]*Instituut-Lorentz, Universiteit Leiden, P. O. Box 9506, 2300 RA Leiden, The Netherlands*
[2]*Institute for Theoretical Physics, KU Leuven, Celestijnenlaan 200D, 3001 Leuven, Belgium*
[3]*Dipartimento di Fisica e Astronomia, Università di Padova, Via Marzolo 8, 35131 Padova, Italy*
[4]*INFN, Sezione di Padova, Via Marzolo 8, 35131 Padova, Italy*
[5]*Institute for Theoretical Physics, Universiteit Utrecht, Leuvenlaan 4, 3584 CE Utrecht, The Netherlands*

The relaxation dynamics of a polymer wound around a fixed obstacle constitutes a fundamental instance of polymer with twist and torque, and it is also of relevance for DNA denaturation dynamics. We investigate it by simulations and Langevin equation analysis. The latter predicts a relaxation time scaling as a power of the polymer length times a logarithmic correction related to the equilibrium fluctuations of the winding angle. The numerical data support this result and show that at short times the winding angle decreases as a power law. This is also in agreement with the Langevin equation provided a winding-dependent friction is used, suggesting that such reduced description of the system captures the basic features of the problem.

PACS numbers: 82.35.Lr

The dynamics of polymers subject to spatial or topological constraints has received quite some attention in recent years. Interesting examples are the translocation of DNA from a narrow pore (for a recent discussion see, e.g., Ref. [1] and references therein) or the dynamics of supercoiled DNA (see, e.g., Ref. [2]). An important question is whether the complex polymer dynamics can be described by a simple equation of motion, using a one-dimensional reaction coordinate. This issue arises, for instance, in the context of polymer translocation (from a pore in a wall) where it was shown that the Langevin equation fails to reproduce simulation results [3]. This failure motivated extensive studies. Various models were put forward, such as the generalized Langevin equation with a memory kernel [4] or a deterministic two-phase model [5].

The aim of this Letter is to study analytically and numerically the unwinding relaxation dynamics, which also belongs to the above class of problems. The equilibrium winding angles for polymers were intensively studied in the past [6–8]. These studies are relevant for a series of problems in physics, e.g., models for the behavior of flux lines in high-T_c superconductors [8]. The relaxation dynamics of unwinding has been much less studied [9,10], though it is a problem of relevance in DNA melting dynamics, but also as a fundamental issue of polymer dynamics involving twist and torsion.

We consider a polymer initially wound around a long impenetrable bar (see Fig. 1), to which it is attached at one end. Because this is an entropically highly unfavorable situation, the polymer will unwind, starting at the loose end; and given enough time, it will relax toward the equilibrium state in which it is no longer winding around the bar. To monitor the unwinding process, we keep track of the winding angle θ of the last monomer of the polymer,

which measures the angle accumulated by the chain around the bar from the first attached monomer to the last free one. We treat the case of polymers with internal excluded volume by studying a self-avoiding walk (SAW) and we support our arguments by also investigating the motion of a random walk (RW). Compared to the more complex unwinding of a double stranded DNA helix, the advantage of dealing with a single polymer around a fixed obstacle is that this winding angle provides a well-defined "reaction coordinate."

The numerical calculations were performed using lattice polymers, specifically L-step RWs on a square lattice and SAWs on a face-centered-cubic (fcc) lattice. An update
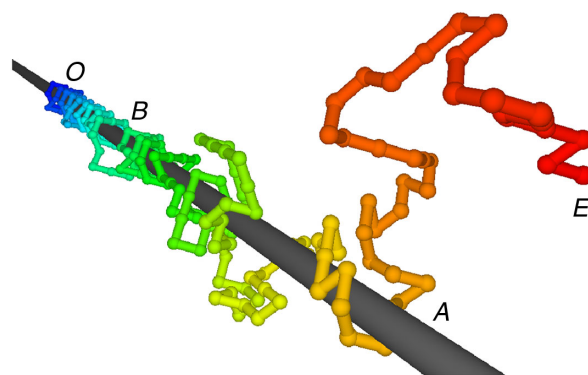

FIG. 1 (color online). Snapshot of a polymer configuration on the fcc lattice, during the unwinding from a bar. The winding angle is defined as $\theta = \sum_{i=1}^{L} \Delta\theta_{i,i+1}$, where $\Delta\theta_{i,i+1}$ is the difference in angles between monomer $i + 1$ and i measured with respect to the bar. The hue follows the monomers order from $i = 1$ (O, attached to the bar, blue online) to $i = L$ (E, red online). The configuration displays a tightly bound helix (OB), a loose helix (BA), and a free end (AE).

consists of a local corner flip or an end-flip move (Rouse dynamics), and a time step includes L attempted updates at random locations. The initial configuration for a RW is constructed by the repetition of a subwalk of 8 monomers winding around the (0,0) site (representing the bar), with a resulting initial winding angle $\theta_0 = \pi L/4$. Similarly, for the SAW on the fcc lattice we repeat a helix formed by 6 steps ($\theta_0 = \pi L/3$) around the bar in the direction [110]. Figure 2 shows a plot of θ vs time in a semilogarithmic scale obtained from numerical simulations: one distinguishes a long-time regime where θ relaxes exponentially and a short-time regime that deviates from the exponential decay. We will discuss the two cases separately.

Our analytical scheme is based on a one-dimensional Langevin equation for the variable θ:

$$\gamma_\tau \frac{d\theta}{dt} = -\frac{\partial \mathcal{F}(\theta, L)}{\partial \theta} + \eta, \qquad (1)$$

with $\mathcal{F}$ the equilibrium free energy for a polymer of length L and winding angle θ, γ_τ the torque friction, and η a noise term. The main focus is on the time evolution of the average winding angle $\langle \theta \rangle$ (indicated with θ for simplicity) and not in fluctuations, so the noise term will be neglected.

The degrees of freedom parallel to the bar are not relevant for a RW and one can restrict the study to a two-dimensional walk, with the bar replaced by an excluded site. For a planar RW the free energy is known exactly [6]:

$$\mathcal{F}_{\mathrm{RW}}(\theta, L) = -k_B T \log\left[\cosh^{-2}\left(\frac{\pi \theta}{\log L} \right) \right]. \qquad (2)$$

For a SAW wound around the bar recent numerical simulations suggest a similar scaling form [11]:
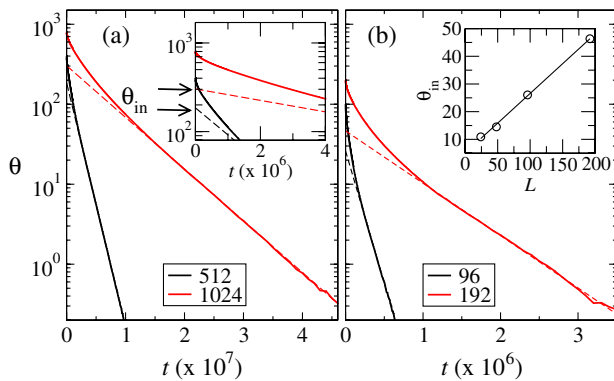

FIG. 2 (color online). Simulations (solid lines) of average winding angles vs time in a semilogarithmic plot for (a) RW in two dimensions and (b) SAW in three dimensions. Only data for two polymer lengths are shown (see legends). Dashed lines are the fit of the exponential decay at long times. Inset of (a): zoom-in of the short-time behavior with extrapolated intercepts θ_{in}. Inset of (b): plot of θ_{in} vs polymer length L, for the SAW data, showing a linear behavior $\theta_{\mathrm{in}} \sim L$.

$$\mathcal{F}_{\mathrm{SAW}}(\theta, L) = -k_B T \log\left[p\left(\frac{\theta}{(\log L)^{0.75}} \right) \right], \qquad (3)$$

where $p()$ is the probability distribution of winding angles obtained from equilibrium Monte Carlo sampling. Here the exponent 0.75 is a numerical estimate [11]. Because both free energies involve a scaling variable $\theta/(\log L)^\alpha$, with $\alpha = 1$ for RWs and $\alpha \approx 0.75$ for SAWs, we can analyze the two processes on equal footing.

We focus first on the longest relaxation time. Equations (2) and (3) are quadratic for small θ. Hence using the lowest-order term and neglecting other proportionality factors, for small angles one obtains an equation of the form

$$\frac{d\theta}{dt} \propto \frac{-\theta}{\gamma_\tau (\log L)^{2\alpha}}. \qquad (4)$$

In order to gain some insights on the L dependence of the torque friction γ_τ one can consider a particle rotating at a fixed distance R from an origin and subject to a constant tangential force f. The Langevin equation in θ is of the form $\gamma_\tau \frac{d\theta}{dt} = \Omega = fR$, where Ω is the torque. The equation can be transformed into a cartesian coordinate $x = R\theta$, yielding

$$f = \frac{\gamma_\tau}{R^2} R\frac{d\theta}{dt} = \frac{\gamma_\tau}{R^2}\frac{dx}{dt} = \gamma \frac{dx}{dt}, \qquad (5)$$

where γ is the friction associated with linear displacement. This implies that $\gamma_\tau = R^2 \gamma$. By integrating over L monomers we obtain $\gamma \sim L$ and hence an average torque friction $\gamma_\tau \sim L^{1+2\nu}$, where the Flory exponent ν describes the average end-to-end squared distance $\langle R^2 \rangle \sim L^{2\nu}$ for a polymer in equilibrium: $\nu = 1/2$ for a RW, while $\nu \simeq 0.588$ for a three-dimensional SAW. Plugging the estimated γ_τ into Eq. (4) one finds the following relaxation time scale:

$$\tau_L \sim L^{1+2\nu}(\log L)^{2\alpha}. \qquad (6)$$

If hydrodynamic effects are included, the friction for linear displacement grows as $\gamma \sim L^\nu$, and the relaxation time becomes $\tau_L \sim L^{3\nu}(\log L)^{2\alpha}$. Note that the leading term of Eq. (6) is similar to the Rouse time $\tau_L^{\mathrm{Rouse}} \sim L^{1+2\nu}$, which is the equilibration time of a free polymer [12]. This is also a lower bound for the unwinding relaxation time, i.e., $\tau_L \gtrsim \tau_L^{\mathrm{Rouse}}$, as the attachment to the bar and its steric hindrance are unlikely to speed up the equilibration process.

In the simulations we determined the total unwinding time τ_L^*, i.e., the average time needed for the unwinding process to be completed. We defined it as the time it takes to reach $\theta = 0$ for the first time. As the polymers are initially wound to $\theta_0 \sim L$, one has to take into account that the relaxation starts from a higher winding angle for longer polymers. The analysis of the numerical data (see Fig. 2) shows that the asymptotic decay is well fitted by $\theta(t) = \theta_{\mathrm{in}} \exp(-t/\tau_L)$ and the intercept θ_{in} scales linearly with L. Hence the condition $\theta(\tau_L^*) \sim 1$ gives

$$\tau_L^* \sim \tau_L \log L \sim L^{1+2\nu}(\log L)^{2\alpha+1}. \qquad (7)$$

Thus, the total unwinding time τ_L^* differs by a factor $\log L$ from the relaxation time scale τ_L.

Plots of $\log \tau_L^*$ vs $\log L$ are shown in Figs. 3(a) (RW) and 3(b) (SAW). In order to analyze the data appropriately we computed $\delta(L)$, defined as the "local" slope in the $\log \tau_L^*$ vs $\log L$ plot for a given size L. Eq. (7) implies

$$\delta(L) \equiv \frac{d \log \tau_L^*}{d \log L} = 1 + 2\nu + \frac{2\alpha+1}{\log L}, \qquad (8)$$

Figures 3(c) and 3(d) (squares) show the numerical estimates of $\delta(L)$ vs $1/\log L$ for the RW and SAW, respectively. The asymptotic scaling predicted by Eq. (8) implies a straight line for $\delta(L)$ when plotted as a function of $1/\log L$ [dashed lines in Figs. 3(c) and 3(d)]. The curvature in the data indicates that further finite-size corrections should be included. In order to rationalize them we introduce a finite-size scaling ansatz $\delta(aL) = 1 + 2\nu + (2\alpha+1)/\log(aL)$ in which an amplitude "a" is included in the logarithmic factor as a single fitting parameter. The best fit of $\delta(aL)$ to the data points produces the two solid lines in Figs. 3(c) and 3(d). The data for the RW [Fig. 3(c)] are in excellent agreement with the ansatz, while the SAW
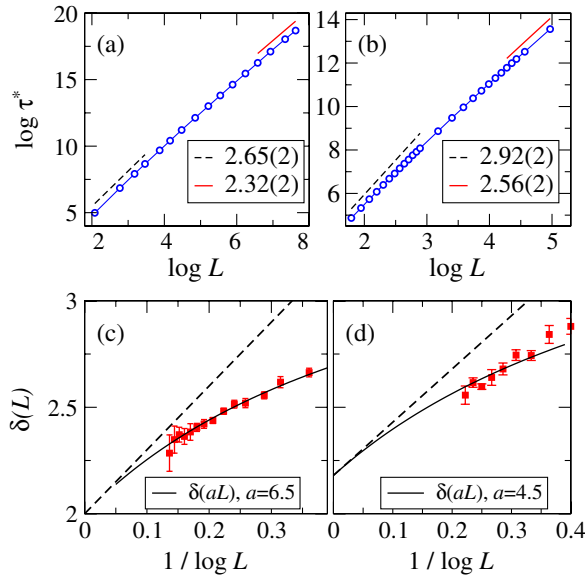

FIG. 3 (color online). (a) Plot of $\log \tau_L^*$ vs $\log L$ for the RW, with lengths up to $L = 2048$. Averages are from 10^4 independent runs for $L < 200$ down to 200 for $L = 1536, 2048$. Dashed and solid lines are fits in the short and long L regimes, showing a systematic variation in the exponent. (b) Same as (a) for SAWs, with lengths up to $L = 144$ (10^5 independent runs per L). (c) Squares: Plot of the RW running exponent $\delta(L)$ obtained from simulations [estimated by a centered difference of data in (a)] as a function of $1/\log L$. Dashed and solid lines represent the scaling $\delta(L)$ and $\delta(a_{RW}L)$, with $a_{RW} = 6.5$, from Eq. (8), respectively. (d) The same for SAWs data from panel (b), with $a_{SAW} = 4.5$.

data are less conclusive: they involve much heavier computations and are thus restricted to much shorter polymers.

We consider next the early-time dynamics of θ. Figure 4 shows a plot of $\theta_0 - \theta(t)$ vs t in log-log scale. For $t \lesssim 10^4$ the data are fitted by a power-law behavior

$$\theta_0 - \theta(t) \sim t^\rho, \qquad (9)$$

with $\rho \approx 0.44$ and $\rho \approx 0.43$ for RW and SAW, respectively. To understand this behavior we consider again the Langevin equation (1). At very high winding, where $\theta(t) \sim \theta_0 \sim L$ the torque due to free energies in Eqs. (2) and (3) are of little use as they describe equilibrium fluctuations for small θ's. In the early stages of the dynamics we expect unwinding only near the free end, regardless of the polymer length. The decrease of θ is then linearly related to the length of the unwound part of the polymer, and to leading order also linearly to the increase in entropy. We thus assume that the torque is constant (L independent), $\tau_0 = -\frac{\partial \mathcal{F}}{\partial \theta} = \text{const}$. At high winding the friction decreases, as the part of the polymer that is tightly wound around the bar does not contribute to it. For $\theta_0 - \theta \ll L$, the friction coefficient should depend only on the difference $\theta_0 - \theta$. Let us consider a friction coefficient vanishing as a power law as $\gamma_\tau(\theta) \sim (\theta_0 - \theta)^x$. Combining this ansatz for γ_τ with the argument for a constant torque τ_0, from Eq. (1) one obtains

$$-\gamma_\tau(\theta)\frac{d\theta}{dt} \sim (\theta_0 - \theta)^x \frac{d}{dt}(\theta_0 - \theta) \sim \tau_0, \qquad (10)$$

which integrated in time, and using the initial condition $\theta(0) = \theta_0$, yields a power-law scaling as that given in Eq. (9) with $\rho = 1/(1+x)$.

To estimate the exponent x we introduce two different types of hypotheses about the shape of the polymer in the early stages of unwinding. These are sketched in Figs. 5(a) and 5(b). In the case of Fig. 5(a), we consider a tightly wound polymer for a length $L - l$ and an unwound loose part of length l and assume that the latter is equilibrated. We denote the winding per unit length in the wound part with $\Delta\omega_1$ and that of the loose part with $\Delta\omega_2$ [$\Delta\omega_2 \approx 0$
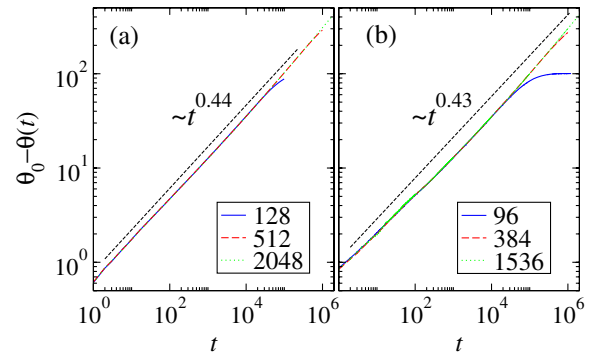

FIG. 4 (color online). $\theta_0 - \theta(t)$ vs t for the RW (a) and the SAW (b). The log-log scale highlights the short-time regime, which behaves as a power law [Eq. (9)] with $\rho \simeq 0.44$ (RW) and $\rho \simeq 0.43$ (SAW).
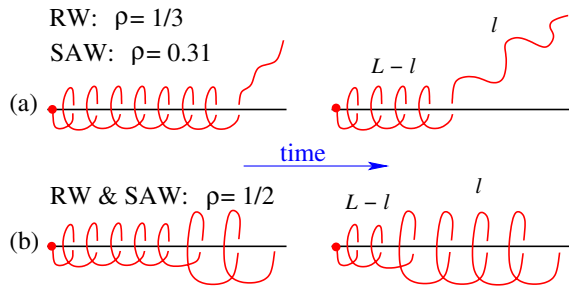
FIG. 5 (color online). Two possible configurations of polymers during unwinding. (a) A tight helix of length $L - l$ connected to a loose equilibrated end of length l. (b) The part of the polymer detached from the bar here still has some winding. The exponents ρ governing the early-time decay of the winding angle predicted in the two cases are given.

in the case of Fig. 5(a)]. The winding angle $\theta = (L - l)\Delta\omega_1 = \theta_0 - l\Delta\omega_1$, hence $\theta_0 - \theta = l\Delta\omega_1$. As shown above in the discussion of the late-time relaxation, an equilibrated polymer of length l has a torque friction scaling as $l^{1+2\nu}$, therefore $\gamma_\tau(\theta) \sim (\theta_0 - \theta)^{1+2\nu}$, which implies $\rho = 1/(2\nu + 2) = 1/3$ for a RW and $\rho = 0.31$ for a SAW. An alternative conformation is shown in Fig. 5(b). In this case we consider a "looser" helix of length l with density of winding per unit length $\Delta\omega_2 > 0$ connected to a tightly wound helix of length $L - l$. Only the former contributes to the friction. In addition, we assume that the looser helix does not change its radius and pitch in time (thus $\Delta\omega_2$ is constant). This seems reasonable at least for the early times of the dynamics. We then have $\theta = (L - l)\Delta\omega_1 + l\Delta\omega_2 = \theta_0 - l(\Delta\omega_1 - \Delta\omega_2)$. As the loose helix maintains its shape while growing the friction is simply proportional to its length: $\gamma_\tau(\theta) \sim l \sim (\theta_0 - \theta)$, which yields $\rho = 1/2$ both for a RW and a SAW.

The conformations of Fig. 5 are of course "idealized" and should represent two extreme cases. In Fig. 5(a) the loose end stretches out from the bar causing a more rapid increase in the friction compared to Fig. 5(b). The exponent $\rho = 1/2$ predicted for the case Fig. 5(b) is quite close to $\rho \approx 0.45$ found in simulations. Snapshots such as that in Fig. 1 suggest that the actual polymer conformations are hybrids of those in Fig. 5. Starting from the free end, one notices a very loose part that does not add much to the winding angle (segment AE in Fig 1). This is reminiscent of the loose equilibrated end of Fig. 5(a). There is then an intermediate part (BA in Fig. 1) wound around the bar, but not tightly, resembling the loose helix of Fig. 5(b).

In conclusion, in this Letter we investigated numerically the relaxation dynamics of polymers wound around a fixed obstacle and we have provided an analytical scheme based on a Langevin equation for the winding angle. Studying such an equation in the late relaxation stage we predict the scaling form of the friction and consequently of the unwinding time scale, which involves logarithmic corrections to the power law of the chain length. The same

equation is also useful in the regime at short times, where a friction depending on the unwinding is needed to describe the observed scaling of the winding angle. The two cases analyzed numerically, a SAW and a RW, provide a consistent picture of the dynamical behavior. Although logarithmic factors are notoriously difficult to study in simulations, finite-size scaling extrapolations of our results are compatible with the predictions of the Langevin equation. It is possible that such strong corrections also affect the unwinding of two polymers from a double-helical conformation. A recent numerical study [10] yields an unwinding time scaling as $\tau_L^* \sim L^{2.58}$; numerically, this scaling is consistent with that of the running exponent found in this work for the longest polymers [see Fig. 3(b)]. It is thus plausible that the relaxation time of an unwinding double helix is also captured by Eq. (7). Besides delving new fundamental aspects of polymer dynamics and providing a reference case for DNA denaturation dynamics, this study may also serve as a basis for other types of investigations involving rotational dynamics, for instance, the relaxation of plectonemic structures that form in overtwisted DNA. Modeling the statics and dynamics of DNA plectonemes has been of recent great interest [2,13–15].

[1] P. Rowghanian and A. Y. Grosberg, J. Phys. Chem. B **115**, 14127 (2011).
[2] A. Crut, D. A. Koster, R. Seidel, C. H. Wiggins, and N. H. Dekker, Proc. Natl. Acad. Sci. U.S.A. **104**, 11 957 (2007).
[3] Y. Kantor and M. Kardar, Phys. Rev. E **69**, 021806 (2004).
[4] D. Panja, G. T. Barkema, and R. C. Ball, J. Phys. Condens. Matter **19**, 432 202 (2007).
[5] T. Sakaue, Phys. Rev. E **81**, 041808 (2010).
[6] J. Rudnick and Y. Hu, Phys. Rev. Lett. **60**, 712 (1988).
[7] B. Duplantier and H. Saleur, Phys. Rev. Lett. **60**, 2343 (1988).
[8] B. Drossel and M. Kardar, Phys. Rev. E **53**, 5861 (1996).
[9] A. Baumgärtner and M. Muthukumar, J. Chem. Phys. **84**, 440 (1986).
[10] M. Baiesi, G. T. Barkema, E. Carlon, and D. Panja, J. Chem. Phys. **133**, 154 907 (2010).
[11] J.-C. Walter, G. T. Barkema, and E. Carlon, J. Stat. Mech.: Theory Exp. (2011) P10020.
[12] M. Doi and S. F. Edwards, *The Theory of Polymer Dynamics* (Oxford University Press, New York, 1989).
[13] B. C. Daniels and J. P. Sethna, Phys. Rev. E **83**, 041924 (2011).
[14] H. Wada and R. R. Netz, Europhys. Lett. **87**, 38 001 (2009).
[15] S. Neukirch and J. F. Marko, Phys. Rev. Lett. **106**, 138104 (2011).